




## Flavonoids as potential therapeutics against novel coronavirus disease-2019 (nCOVID-19)

Gourav Rakshit, Pankaj Dagur, Swaha Satpathy, Arjun Patra, Alok Jain & Manik Ghosh


To cite this article: Gourav Rakshit, Pankaj Dagur, Swaha Satpathy, Arjun Patra, Alok Jain & Manik Ghosh (2021): Flavonoids as potential therapeutics against novel coronavirus disease-2019 (nCOVID-19), Journal of Biomolecular Structure and Dynamics, DOI: [10.1080/07391102.2021.1892529](https://doi.org/10.1080/07391102.2021.1892529)

To link to this article: <https://doi.org/10.1080/07391102.2021.1892529>

 [View supplementary material](#) 

 Published online: 08 Mar 2021.





 [Submit your article to this journal](#) 

 [View related articles](#) 

 [View Crossmark data](#) 



## Flavonoids as potential therapeutics against novel coronavirus disease-2019 (nCOVID-19)

Gourav Rakshit<sup>a\*</sup> , Pankaj Dagur<sup>a\*</sup> , Swaha Satpathy<sup>b</sup> , Arjun Patra<sup>c</sup> , Alok Jain<sup>d</sup>  and Manik Ghosh<sup>a</sup> 

<sup>a</sup>Department of Pharmaceutical Sciences and Technology, Birla Institute of Technology, Ranchi, Jharkhand, India; <sup>b</sup>Department of Biotechnology and Bioinformatics, Sambalpur University, Sambalpur, Odisha, India; <sup>c</sup>Department of Pharmacy, Guru Ghasidas University, Bilaspur, Chhattisgarh, India; <sup>d</sup>Department of Bio-Engineering, Birla Institute of Technology, Ranchi, Jharkhand, India

Communicated by Ramaswamy H. Sarma

### ABSTRACT

Since time immemorial natural products have been a great source of medicine to mankind. The anti-viral activities from several ayurvedic herbal medicines (in the form of crude extract or fraction or isolated compounds) have been established but their effectiveness against coronavirus still needs to be explored. They can provide a rich resource of anti-SARS-CoV-2 drug candidates. In this paper, *in-silico* techniques have been used to identify the potential lead molecules against SARS-CoV-2. A list of flavonoids having anti-viral activity was prepared and evaluated against the selected target. Rhoifolin, 5,7-dimethoxyflavanone-4'-O- $\beta$ -d-glucopyranoside, baicalin, astragaloside, luteolin, and kaempferol showed good binding affinity and thus these could be promising compounds. *In-silico* screening such as ADMET prediction has been performed which predicted that the selected flavonoids have good pharmacokinetics and pharmacodynamics properties. Molecular dynamics simulation studies and MM-PBSA binding free energy calculations showed luteolin to be a more effective candidate against viral protein Mpro. The novelty of the approach mainly rests in the identification of potent anti-viral natural molecules from natural products flavonoid group of molecules to be effective against the latest coronavirus infection.

### ARTICLE HISTORY

Received 21 August 2020  
Accepted 15 February 2021

### KEYWORDS






COVID-19; flavonoids; *in-silico*; ADMET; molecular dynamics; MM-PBSA

## 1. Introduction


COVID-19 (caused by SARS-CoV-2) is a highly infectious disease that originated in Wuhan, China, and was later declared as a global emergency and pandemic (in March 2020) by World Health Organization (WHO) (Sohrabi et al., 2020). Tracing through the history of coronaviruses, its first family member was discovered in the 1930s but it gained popularity in the year 2002–03 when a severe acute respiratory syndrome (SARS) outbreak joggled the world by its severity (Hui et al., 2003). After a decade later in 2012, it made hark back and was diagnosed in Saudi Arabia in the form of the Middle East respiratory syndrome (MERS), also known as camel flu which was believed to be originated from bats but humans had been typically infected from camels, either during direct contact or indirectly (Chafekar & Fielding, 2018). Lastly, it emerged as novel coronavirus disease-2019 (nCOVID-19) (Rothan & Byrareddy, 2020). As of January 27, 2021, there have been 99,363,697 confirmed cases of COVID-19, including 2,135,959 deaths as per reports of WHO (World Health Organization, 2021). In India, as of January 27, 2021, a total of 10,690,281 confirmed cases have been reported out

of which 173,733 are active; 10,358,328 recovered; and 153,751 deaths (COVID19INDIA 2020).

Currently, no specific treatment is available for this dreadful disease as the proliferation and pathogenesis of the virus is not clear. The medicines used for this disease are mainly based on their effectiveness against other strains of coronavirus such as SARS-CoV and MERS-CoV. During the path of drug development some drug molecules, either single or in combination, have been screened against the virus, which exhibited the effect through various mechanisms. The different mode of actions of biomolecules against the virus includes rebalancing Renin-Angiotensin System (RAS), binding to SARS-CoV-2 M<sup>Pro</sup>, binding to SARS-CoV-2 protease, binding to angiotensin II human acetate, binding to SARS-CoV-2 3C-like proteinase (3CL<sup>Pro</sup>), binding to SARS-CoV-2 papain-like proteinase (PL<sup>Pro</sup>), binding to AP2-associated protein kinase 1 (AAK1), etc. (Rismanbaf, 2020). In elderly people, some other disease conditions like hypertension, diabetes mellitus, and coronary heart disease enhance the vulnerability to COVID-19 (Danser et al., 2020). This is because the ACE2 receptor allows coronavirus entry into cells and prior use of RAS blockers might have a high risk of SARS-CoV-2

**CONTACT** Manik Ghosh  manik@bitmesra.ac.in  Department of Pharmaceutical Sciences and Technology, Birla Institute of Technology, Ranchi, Jharkhand 835215, India; Alok Jain  alokjain@bitmesra.ac.in  Department of Bio-Engineering, Birla Institute of Technology, Ranchi, Jharkhand 835215, India; Arjun Patra  drarjunpatra22@gmail.com  Department of Pharmacy, Guru Ghasidas University, Bilaspur, Chhattisgarh, India.

\*Gourav Rakshit and Pankaj Dagur Equal contribution.

 Supplemental data for this article can be accessed online at <https://doi.org/10.1080/07391102.2021.1892529>.

© 2021 Informa UK Limited, trading as Taylor & Francis Group

infection. Binding of the virus to the ACE2 receptor needs viral spike protein (S1) and then the cell entry depends on priming by the serine protease TMPRSS2 (transmembrane protease, serine 2) (Li et al., 2003; Matsuyama et al., 2010). SARS-CoV-2 can also enter the cell through this route (Hoffmann et al., 2020; Zhou et al., 2020). It is postulated based on the currently available evidence that treatment with RAS blockers, ACE inhibitors should be continued to stable patients with coronavirus infection (Danser et al., 2020; Meili et al., 2020). The RAS blockers could be a better option for the treatment of COVID-19 pneumonia (Kreutz et al., 2020). The COVID-19 is here to stay as the common flu for years to come even after successful vaccines. The need of the hour is to develop/identify some drug molecules for the effective treatment of this highly emerging devastating disease. Nature has always some remedy for a disease condition and natural products have been found to possess therapeutic benefits for various ailments. Considering the RAS blockers are beneficial in the management of coronavirus infection and the usefulness of flavonoids as antiviral agents, we have selected some flavonoids for molecular docking study with SARS-CoV-2 main protease ( $M^{pro}$ ). The selected flavonoids have been reported as RAS inhibitors (Yang et al., 2019) and have antiviral properties (Sawikowska, 2020; Zakaryan et al., 2017). As mentioned earlier, many targets are available for treating COVID-19, but  $M^{pro}$  is selected in the curiosity to treat infected patients by inhibition/stop of viral infection in the cell (Enmozhi et al., 2020; Jin et al., 2020).

## 2. Materials and methods

### 2.1. Hardware and software employed

Docking part of current study was done using an HP workstation equipped with Windows 8 single language (64 bit operating system), intel (R) Core™ i3-3110M CPU @ 2.40 GHz processor system, installed memory (RAM) of 4GB, the hard disk drive of 1TB. Software used were autodock-4.2.6 program along with MGLtools-1.5.6 for the docking purpose (Rizvi et al., 2013), chemdraw15.0 (Perkin-Elmer) for sketching and preparation of ligand. Visualizations were done using UCSF Chimera1.13.1 (Pettersen et al., 2004). LigPlot<sup>+</sup> and BIOVIA Discovery Studio Visualizer programs were used for the generation of 2D ligand-protein interaction diagrams (Laskowski & Swindells, 2011). Online resources used were: protein data bank (Berman et al., 2000), molprobit server for protein preparation (Williams et al., 2017), molinspiration, and PRODRG server for ligand preparation (van Aalten et al., 1996).

### 2.2. Docking studies

#### 2.2.1. Protein structure preparation

The crystal structure of COVID-19 main protease (PDB ID: 6LU7) was selected for the study (Jin et al., 2020). The 3D X-ray crystallographic structures were downloaded from protein data bank (PDB) and prepared in the MOLPROBITY server. Preparation involved fetching the protein from the

server by calling the PDB ID, uploading the molecule, adding hydrogens to it, applying selected flips to residues, analyzing all-atom contacts and geometry, running the job, and downloading the final protein file.

#### 2.2.2. Ligand preparation

The ligand molecules/compounds used in this study are mentioned in Table 1. The respective individual structures were drawn using Chemdraw15.0 and then visualized using Chem3D15.0. PRODRG server was used for ligand preparation (van Aalten et al., 1996). Preparation involved putting the PDB coordinates of the ligand and running the job. The final stabilized structure was auto-downloaded from the server and it was saved for protein-ligand docking.

#### 2.2.3. Validation of docking procedure

Validation of the crystal structure of COVID-19 main protease (PDB ID: 6LU7) from synthetic construct in complex with an inhibitor N3 was performed by redocking co-crystallized ligand N-[(5-methylisoxazol-3-yl)carbonyl]alanyl-l-valyl-n~1~((1r,2z)-4-(benzyloxy)-4-oxo-1-[(3r)-2-oxopyrrolidin-3-yl]methyl}but-2-enyl)-l-leucinamide (PRD\_002214) into the respective active site/binding site. The grid coordinates were noted for further reference.

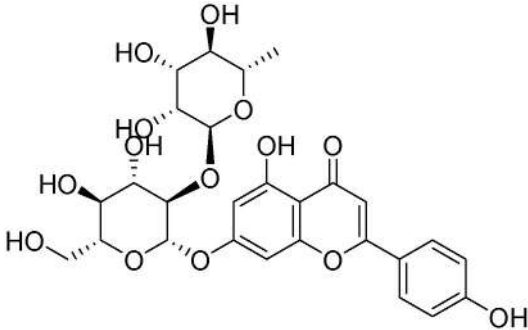
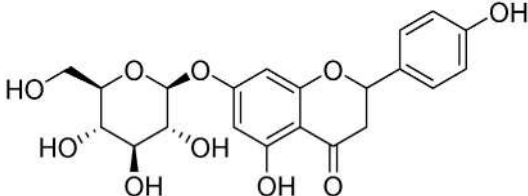
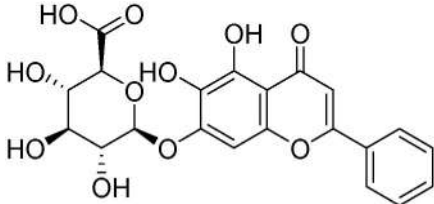
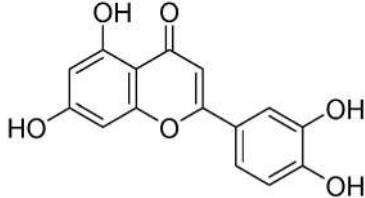
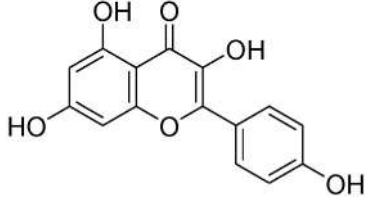
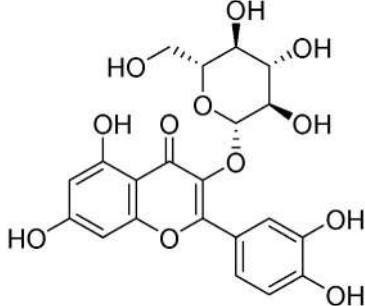
#### 2.2.4. Protein-ligand docking

All molecular docking studies were performed using the Autodock-4.2.6 program (ADP) (Rizvi et al., 2013). Protein and ligands were prepared using ADP tools. In grid settings, the grid box dimensions were 60x60x60 in x, y, and z directions, and coordinate values were taken from re-docking studies. Grid point spacing was 0.375 Å in each case. Auto grid-4.2 was used for generating map files. A genetic algorithm (GA) was used for search parameters. The number of GA run was 50, the number of evaluations was 2,500,000 and the population size was 150. The final procedure involved the running of the auto grid and auto dock. Auto grid-4.2 was used for generating map files and Autodock-4.2 was used for running molecular docking of each ligand on respective protein. All docking data were analyzed, and visualizations of various structures were done using Autodock-4.2 along with MGLTools-1.5.6.

### 2.3. ADME prediction


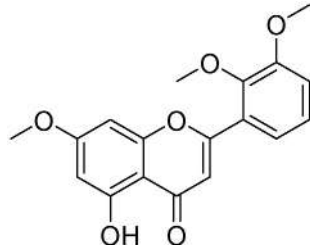
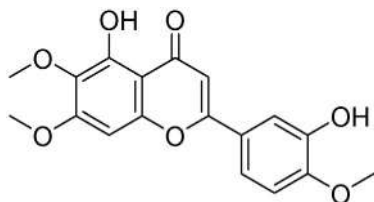
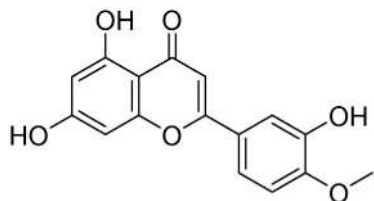
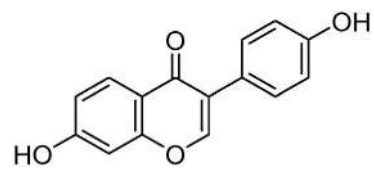
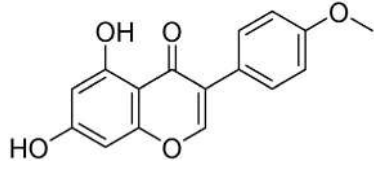
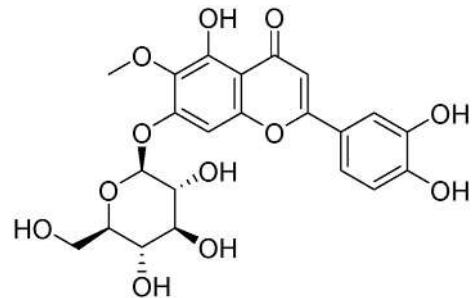
ADME (absorption, distribution, metabolism, and excretion) is a key aspect to predict the pharmacodynamics of the molecule under study which could be used as a future lead molecule for drug development. SWISSADME is an online web server developed and maintained by the molecular modeling group of the Swiss Institute of Bioinformatics (SIB) (<https://www.swissadme.ch>). To compute ADME parameters, already prepared structures of ligands/molecules were uploaded individually in the Marvin JS section provided on the website <http://swissadme.ch/index.php>. Structures were auto

**Table 1.** List of top 15 selected flavonoids for the study with their code and structure.

Code	Name of flavonoid	Structure
FL01	Rhoifolin	
FL02	5,7dimethoxyflavanone-4'-O-beta-glucopyranoside	
FL03	Baicalin	
FL04	Luteolin	
FL05	Kaempferol	
FL06	Isoquercetin	

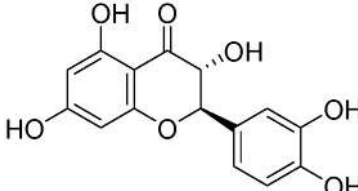
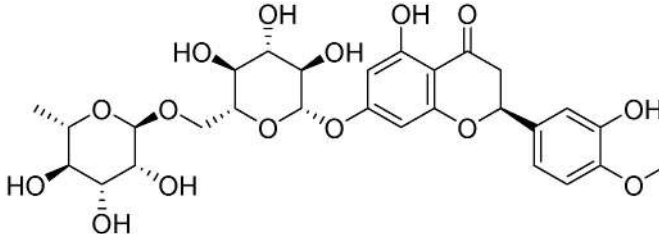
(continued)

Table 1. Continued.

Code	Name of flavonoid	Structure
FL07	Tamarixetin	
FL08	5-Hydroxy-3,4,7-trimethoxy-flavonone	
FL09	Eupatorine	
FL10	Diosmetin	
FL11	Daidzein	
FL12	Biochanin A	
FL13	Nepitrin	

(continued)

Table 1. Continued.

Code	Name of flavonoid	Structure
FL14	Taxifolin	
FL15	Hesperidin	

converted to SMILES format and then ADME was predicted by the server. Results obtained were saved for further analysis.

#### 2.4. Toxicity prediction

Prediction of toxicity is an important aspect of all molecules. PkCSM is a web server database in which analysis of molecules is done by drawing the small molecule virtually or by submitting the SMILES format of the same. The web server database provides details of toxicity namely AMES toxicity, maximum tolerated dose, hepatotoxicity, skin sensitization, hERG I, and II inhibitor. The website was logged on and the SMILES of the top score molecules after docking were searched and submitted into the website and toxicity was selected in prediction mode (Pires et al., 2015).

#### 2.5. Molecular dynamics and simulations

Molecular dynamics (MD) simulation studies were carried out on the MPro (PDB ID: 6LU7) with the top two best compounds based on the above-mentioned analysis. Groningen Machine for Chemical Simulations (GROMACS); v. 2019.4 (using GROMOS 54A7 force field for protein) (Abraham et al., 2015; Van Der Spoel et al., 2005) was used to perform MD simulation studies. 'pdb2gmx' module was used to prepare the protein topology, while the ligands force field parameters were generated from Automatic Topology Builder (ATB) (Malde et al., 2011). Complex structures were solvated with 31,690 single point charge (SPC/E) water model (Mark & Nilsson, 2001) in a cubical box. Both the systems were neutralized by adding the counter ions if needed. Steepest descent followed by conjugate gradient minimization algorithms was employed to achieve minimized energy structures. Energy minimized structures were subjected to two steps equilibration run. During the first equilibration phase, all the heavy atoms of the proteins were positioned restrained for 2 ns in the NVT ensemble to settle down the solvent molecules. In the second equilibration run, all the positioned restrained were removed and run for 2 ns in the NPT ensemble. LINCS and

SETTLE algorithm were employed to constrain the covalent bonds and water hydrogen in the system (Hess et al., 1997; Miyamoto & Kollman, 1992). Particle mesh Ewald method (1.4 nm cut-off and 0.16 Fourier spacing) was adopted to calculate the long-range electrostatic interactions (Essmann et al., 1995). Short-range interactions were truncated at 1.4 nm. Periodic boundary conditions were applied in all three directions. The temperature and pressure of the system were regulated by the V-rescale weak coupling (Berendsen et al., 1984) and Parrinello Rahman method (Parrinello & Rahman, 1981) algorithms at 300 K and 1 bar, respectively. Finally, the well-equilibrated complexes without any restraint were run it for a 120 ns and considered as production phase. Using the various inbuilt modules of the GROMACS simulation suit the various analyses were performed on the produced trajectories of MD simulations.

##### 2.5.1. MM-PBSA calculations

Molecular Mechanic/Poisson-Boltzmann Surface Area (MM-PBSA) gives the binding free energy of protein and ligand complexes and extensively used in the past (Rastelli et al., 2010; Weis et al., 2006). The molecular interactions that occur between protein and ligand are provided by the binding free energies which have contributions from molecular mechanics potential energy, polar and non-polar solvation energies. Molecular mechanics potential constitutes the bonded and non-bonded energy terms. The free energy of binding was computed for full 120 ns simulations by utilizing the 'g\_mmpbsa' module (Kumari et al., 2014). All the energy components were calculated for the structures saved at every 500 ps time interval. The binding energy was calculated by employing the equation given below:

$$\Delta G_{\text{binding}} = G_{\text{complex}} - (G_{\text{receptor}} + G_{\text{ligand}})$$

$\Delta G_{\text{binding}}$  depicts the binding energy of the complex,  $G_{\text{receptor}}$  shows the free receptor's binding energy, and  $G_{\text{ligand}}$  represents the unbounded ligand's binding energy.

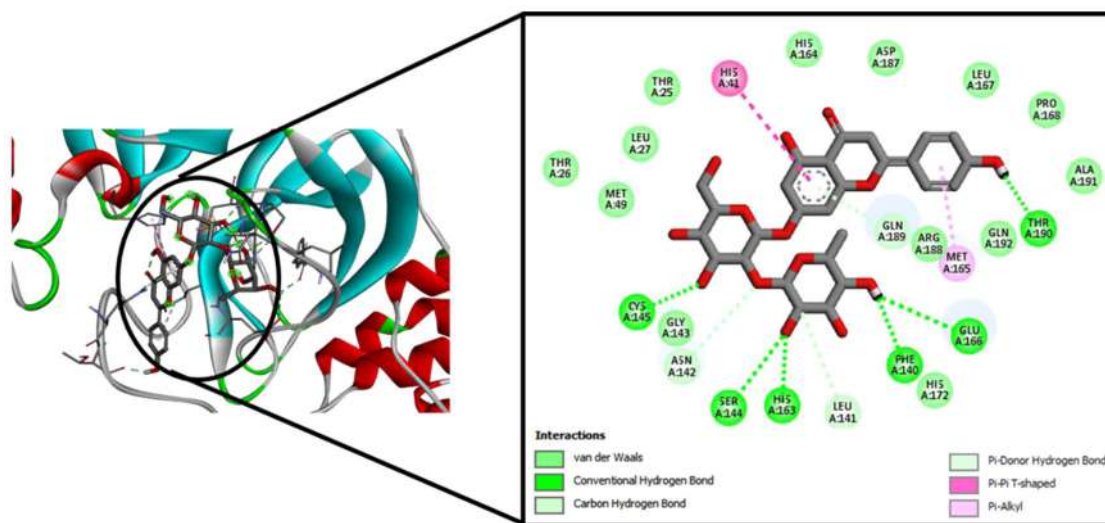


**Table 2.** Details of docking-based parameters of identified potential flavonoids in the binding pocket of target protein, COVID-19 main protease (PDB ID: 6LU7).

S. No/Code	Ligands	1st Run		2nd Run		3rd Run	
		Binding energy	Inhibition constant	Binding energy	Inhibition constant	Binding energy	Inhibition constant
1	Internal Ligand	-7.26	4.77 $\mu$ M	-7.07	6.55 $\mu$ M	-7.04	6.86 $\mu$ M
FL01	Rhoifolin	-9.28	156.4 nM	-7.86	1.74 $\mu$ M	-7.49	3.26 $\mu$ M
FL02	5,7-dimethoxyflavanone-4'-O- $\beta$ -d-glucopyranoside	-8.81	348.25 nM	-8.21	960.39 nM	-7.48	3.26 $\mu$ M
FL03	Baicalin	-8.29	843.68 nM	-6.79	10.61 $\mu$ M	-6.67	12.8 $\mu$ M
FL04	Luteolin	-8.14	1.08 $\mu$ M	-8.13	1.09 $\mu$ M	-8.13	1.1 $\mu$ M
FL05	Kaempferol	-8.11	1.13 $\mu$ M	-8.05	1.25 $\mu$ M	-8.02	1.32 $\mu$ M
FL06	Isoquercetin	-8.02	1.32 $\mu$ M	-7.85	1.78 $\mu$ M	-7.75	2.07 $\mu$ M
FL07	Tamarixetin	-7.81	1.88 $\mu$ M	-7.7	2.25 $\mu$ M	-7.69	2.32 $\mu$ M
FL08	5-Hydroxy-3,4,7-trimethoxy-flavonone	-7.76	2.04 $\mu$ M	-7.76	2.06 $\mu$ M	-7.76	2.07 $\mu$ M
FL09	Eupatorine	-7.69	2.31 $\mu$ M	-7.38	3.87 $\mu$ M	-7.33	4.24 $\mu$ M
FL10	Diosmetin	-7.57	2.85 $\mu$ M	-7.55	2.93 $\mu$ M	-7.5	3.17 $\mu$ M
FL11	Daidzein	-7.47	3.37 $\mu$ M	-7.46	3.38 $\mu$ M	-7.45	3.47 $\mu$ M
FL12	Biochanin A	-7.2	5.29 $\mu$ M	-7.19	5.35 $\mu$ M	-7.18	5.44 $\mu$ M
FL13	Nepitrin	-6.61	14.34 $\mu$ M	-6.21	27.95 $\mu$ M	-5.59	80.28 $\mu$ M
FL14	Taxifolin	-6.29	24.5 $\mu$ M	-6.21	27.91 $\mu$ M	-6.13	31.98 $\mu$ M
FL15	Hesperidin	-6.22	27.63 $\mu$ M	-5.08	189.64 $\mu$ M	-4.65	388.12 $\mu$ M

**Table 3.** Details of top score identified potential flavonoids showing H-bond interacting residues in the binding pocket of COVID-19 main protease (PDB ID: 6LU7).

Code	Ligands	H-bond residues	H-bond distance ( $\text{\AA}$ )
FL01	Rhoifolin	Cys145, Ser144, His163, Phe140, Glu166, Thr190	2.046, 2.248, 2.444, 2.232, 2.682, 1.774
FL02	5,7-dimethoxyflavanone-4'-O- $\beta$ -d-glucopyranoside	Thr190, Leu141, Asn142	2.054, 2.239, 2.264
FL03	Baicalin	Gly143, Ser144, Asn142, Glu166	2.118, 2.252, 2.034, 2.151
FL04	Luteolin	Thr190, Glu166, Asp187	2.031, 1.921, 1.913
FL05	Kaempferol	Thr190, Asp187, His164	2.028, 2.122, 2.038

**Figure 1.** Docking interaction of rhoifolin in the binding pocket of COVID-19 main protease (PDB ID: 6LU7) showing six hydrogen bonds.

### 3. Results

#### 3.1. Docking studies

##### 3.1.1. Validation of the model

The validation model of protein (PDB ID: 6LU7) revealed that the binding energy was  $-7.26$  kcal/mol with pKi of  $4.77 \mu$ M and reference RMSD of  $2.45 \text{\AA}$ .

##### 3.1.2. Docking

The docking investigation of all the ligands with SARS-CoV-2 main protease exhibited favorable binding energies and

inhibition constants. Top score compounds namely rhoifolin ( $-9.28$ ,  $156.4$  nM), 5,7-dimethoxyflavanone-4'-O- $\beta$ -d-glucopyranoside ( $-8.81$ ,  $348.25$  nM), baicalin ( $-8.29$ ,  $843.68$  nM), luteolin ( $-8.14$ ,  $1.08 \mu$ M) and kaempferol ( $-8.11$ ,  $1.13 \mu$ M) indicated a high affinity for the binding pocket and had high negative binding energies and low inhibition constants as compared to the internal ligand ( $-7.26$ ,  $4.77 \mu$ M). The binding energies/docking scores and inhibition constants of all molecules are given in Table 2.

The binding conformations of the top score five compounds in the active binding pocket involved H-bond interactions with residues of the interacting protein. The details

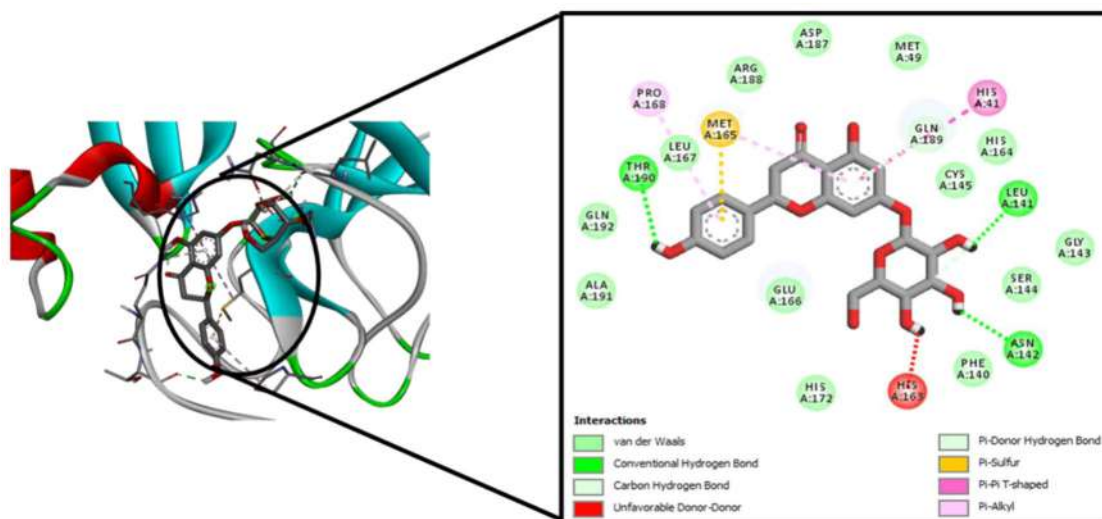


Figure 2. Docking interaction of 5,7-dimethoxyflavanone-4'-O- $\beta$ -d-glucopyranoside in the binding pocket of COVID-19 main protease (PDB ID: 6LU7) showing three hydrogen bonds.

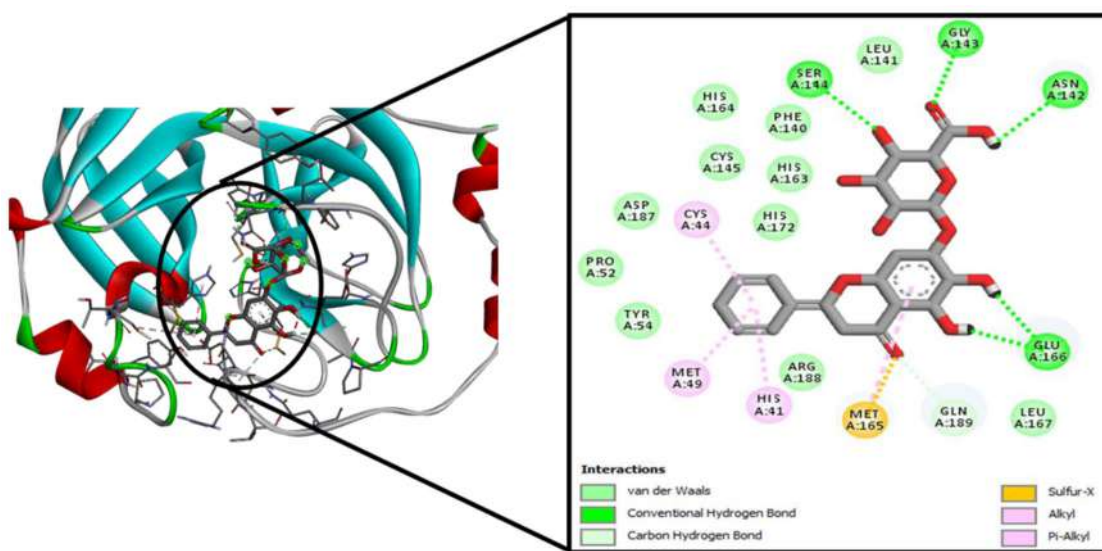


Figure 3. Docking interaction of baicalin in the binding pocket of COVID-19 main protease (PDB ID: 6LU7) showing four hydrogen bonds.

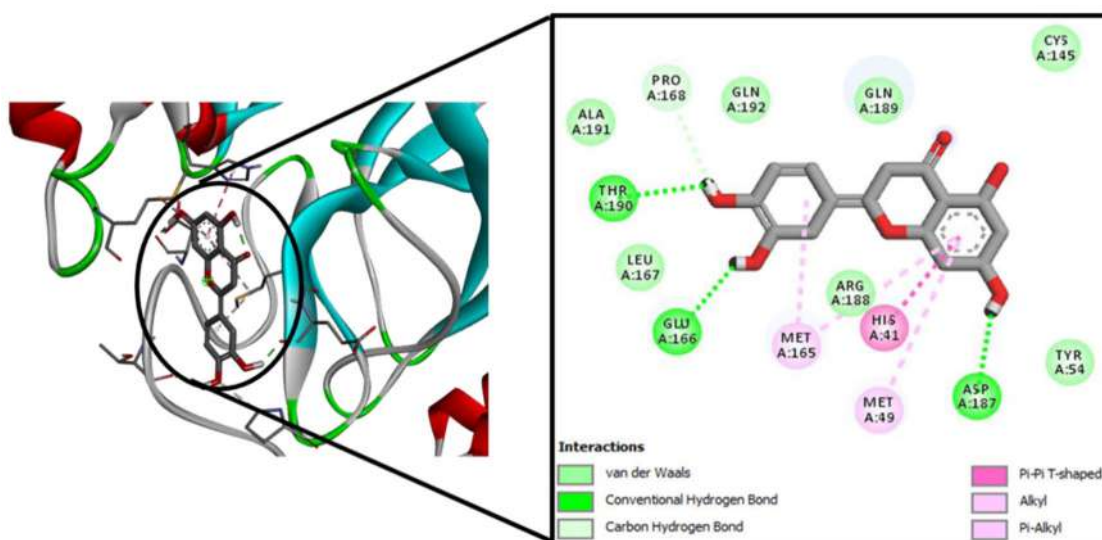
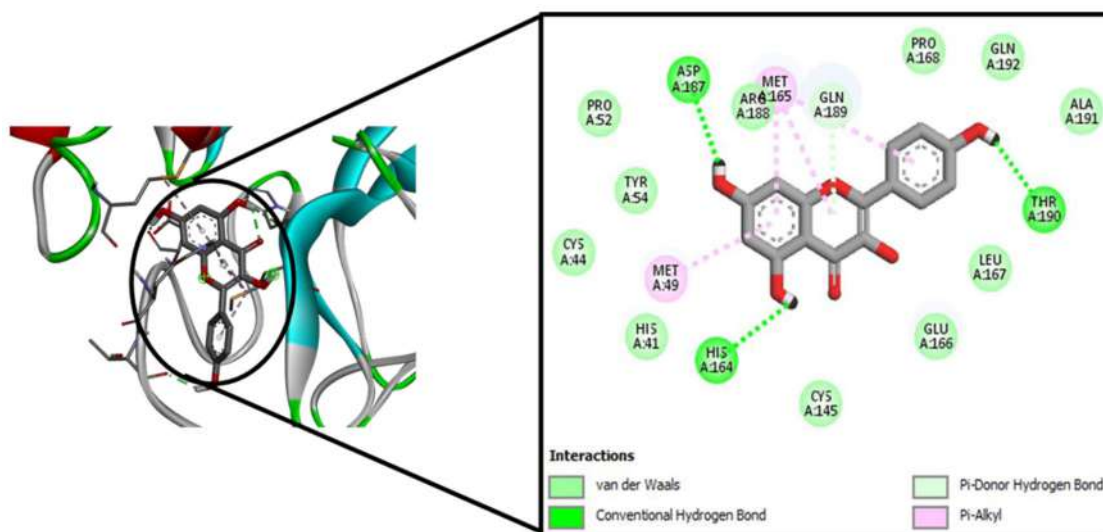
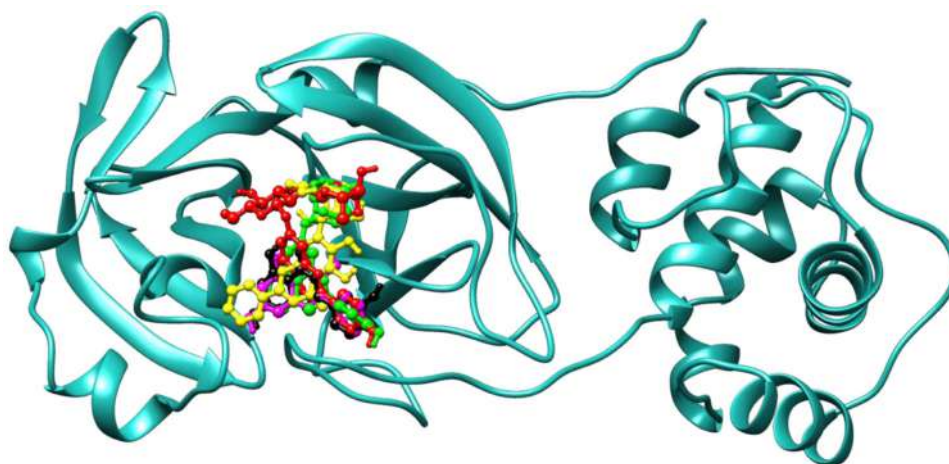


Figure 4. Docking interaction of luteolin in the binding pocket of COVID-19 main protease (PDB ID: 6LU7) showing three hydrogen bonds and one  $\pi$ - $\pi$  interaction.





**Figure 5.** Docking interaction of kaempferol in the binding pocket of COVID-19 main protease (PDB ID: 6LU7) showing three hydrogen bonds.



**Figure 6.** Superimposed structures of top score identified potential flavonoids in the binding pocket of COVID-19 main protease. Baicalin, 5,7-dimethoxyflavanone-4'-O- $\beta$ -d-glucopyranoside, kaempferol, luteolin and rhoifolin are shown in yellow, green, magenta, black, and red color, respectively. Protein (PDB ID: 6LU7) is displayed in carton representation. Hydrogen atoms are not shown for clarity.

of the residues involved in bonding with ligands i.e. H-bond interactions residues with distances are given in Table 3 and the docking images are shown in Figures 1–5. Figure 6 shows the superimposed image of top score five identified potential flavonoids along with internal ligand in the binding pocket of COVID-19 main protease (PDB ID: 6LU7) showing conserved hydrogen bonding. SwissADME web server database that was used came with the results after submission of the compounds/ligands.

### 3.2. ADME prediction

#### 3.2.1. Results of drug-likeness, bioavailability, synthetic feasibility, and alerts for PAINS & Brenk filters

Drug-likeness refers to the probability of a compound to become an oral drug regarding its bioavailability. Five different filters were employed to calculate the drug-likeness for our fifteen sets of query compounds as represented in Table 4. The results exhibited that eight compounds (FL04, FL05, FL07, FL09, FL10, FL11, FL12, and FL14) revealed a

good drug-likeness score with zero violation of drug-likeness rules and exhibited a lead-likeness with no violation. PAINS and Brenk methods were employed to recognize the possible uncertain fragments that yield false-positive biological output. The results of which revealed that compounds FL03, FL04, FL06, FL13, and FL14 showed violation due to the inclusion of fragment catechol. The rest of the compounds did not show violations. The lead likeness was also calculated for the compounds along with the synthetic accessibility appraisal. The compounds that showed high scores were removed as they were tough to synthesize as per protocols. The obtained results revealed that these eight compounds (FL04, FL05, FL07, FL09, FL10, FL11, FL12, and FL14) could be synthesized easily as their score was in the range of 2.79–3.51. The Abbot bioavailability score prognosticates the fate of a molecule to have 10% oral bioavailability (in rat) or quantifiable Caco-2 cell line permeability experiment and may be defined by a feasibility score of 11%, 17%, 56%, and 85%. Our eight compounds exhibited a score of 56%, defining good bioavailability.

**Table 4.** Tabular representation of different drug-likeness rules, bioavailability, lead-likeness, synthetic accessibility, and alerts for PAINS and Brenk.

Code	Compound	Drug-likeness Rules					Bioavailability Score	Alerts		Lead likeness	Synthetic Accessibility
		Lipinski (Pfizer)	Ghose (Amgen)	Veber (GSK)	Egan (Pharmacia)	Muege (Bayer)		PAINS	Brenk		
FL01	Rhoifolin	No	No	No	No	No	0.17	0	0	No	6.33
FL02	5,7-dimethoxyflavanone-4'-O- $\beta$ -d-glucopyranoside	Yes	Yes	No	No	No	0.55	0	0	No	4.98
FL03	Baicalin	No	Yes	No	No	No	0.11	Catechol_A	Catechol	No	5.09
FL04	Luteolin	Yes	Yes	Yes	Yes	Yes	0.55	Catechol_A	Catechol	Yes	3.02
FL05	Kaempferol	Yes	Yes	Yes	Yes	Yes	0.55	0	0	Yes	3.14
FL06	Isoquercetin	No	No	No	No	No	0.17	Catechol_A	Catechol	No	5.32
FL07	Tamarixetin	Yes	Yes	Yes	Yes	Yes	0.55	0	0	Yes	3.26
FL08	5-Hydroxy-3,4,7-trimethoxy-flavonone	Yes	Yes	Yes	Yes	Yes	0.55	0	0	No	3.43
FL09	Eupatorine	Yes	Yes	Yes	Yes	Yes	0.55	0	0	Yes	3.43
FL10	Diosmetin	Yes	Yes	Yes	Yes	Yes	0.55	0	0	Yes	3.05
FL11	Daidzein	Yes	Yes	Yes	Yes	Yes	0.55	0	0	Yes	2.79
FL12	Biochanin A	Yes	Yes	Yes	Yes	Yes	0.55	0	0	Yes	2.89
FL13	Nepitrin	No	Yes	No	No	No	0.17	Catechol_A	Catechol	No	5.36
FL14	Taxifolin	Yes	Yes	Yes	Yes	Yes	0.55	Catechol_A	Catechol	Yes	3.51
FL15	Hesperidin	No	No	No	No	No	0.17	0	0	No	6.34

**Table 5.** Details of in-silico ADME profile of eight selected flavonoids using Swiss ADME online server.

		FL04	FL05	FL07	FL09	FL10	FL11	FL12	FL14
A	Physiochemical Formula	C <sub>15</sub> H <sub>10</sub> O <sub>6</sub>	C <sub>15</sub> H <sub>10</sub> O <sub>6</sub>	C <sub>16</sub> H <sub>12</sub> O <sub>7</sub>	C <sub>16</sub> H <sub>16</sub> O <sub>7</sub>	C <sub>16</sub> H <sub>12</sub> O <sub>6</sub>	C <sub>15</sub> H <sub>10</sub> O <sub>4</sub>	C <sub>16</sub> H <sub>12</sub> O <sub>5</sub>	C <sub>15</sub> H <sub>12</sub> O <sub>7</sub>
D	parameters Molecular weight	286.24 g/mol	286.24 g/mol	316.26 g/mol	344.32 g/mol	300.26 g/mol	254.24 g/mol	284.26 g/mol	304.25 g/mol
M	Mol. refractivity	76.01	76.01	82.50	91.44	80.48	71.97	78.46	74.76
E	TPSA	111.13 Å <sup>2</sup>	111.13 Å <sup>2</sup>	120.36 Å <sup>2</sup>	98.36 Å <sup>2</sup>	100.13 Å <sup>2</sup>	70.67 Å <sup>2</sup>	79.90 Å <sup>2</sup>	127.45 Å <sup>2</sup>
T	Lipophilicity ILOGP	1.86	1.70	2.24	3.07	2.47	1.77	2.55	0.71
	SILICOS-IT	2.03	2.03	2.06	3.12	2.55	3.02	3.03	0.66
	Water solubility Log S (ESOL), Class	-3.71	-3.31	-4.04	-4.33	-4.06	-3.53	-3.92	-2.66
P	Log S (Ali), Class	-4.51	-3.86	-5.14	-5.14	-4.87	-3.60	-4.33	-3.21
R	SILICOS-IT, Class	-3.82	-3.82	-3.94	-5.33	-4.52	-4.98	-5.10	-2.03
O	Pharmacokinetics GI absorption	High	High	High	High	High	High	High	High
F	BBB permeant	No	No	No	No	No	Yes	No	No
I	Log K <sub>p</sub> (skin perm.)	-6.25 cm/s	-6.70 cm/s	-6.13 cm/s	-5.99 cm/s	-5.93 cm/s	-6.10 cm/s	-5.91 cm/s	-7.48 cm/s
L	CYP1A2	Yes	Yes	Yes	Yes	Yes	Yes	Yes	No
E	CYP2C19	No	No	No	No	No	No	No	No
	CYP2C9	No	No	Yes	Yes	Yes	No	No	No
	CYP2D6	Yes	Yes	Yes	Yes	Yes	Yes	Yes	No
	CYP3A4	Yes	Yes	Yes	Yes	Yes	Yes	Yes	No

### 3.2.2. In-silico evaluation of pharmacokinetics compliance

The fulfillment of a drug's journey in the whole body is evaluated in terms of ADME (absorption, distribution, metabolism, and elimination). The ADME parameters were calculated for compounds under study, i.e. FL04, FL05, FL07, FL09, FL10, FL11, FL12, and FL14 by calculating the different physicochemical and bio-pharmaceutical highlights. After accessing the physiochemical features for different flavonoids, the results indicated that the molecular refractivity was 76.01, 76.01, 82.50, 91.44, 80.48, 71.97, 78.46, and 74.76 while the topological polar surface area (TPSA) was 111.13 Å<sup>2</sup>, 111.13 Å<sup>2</sup>, 120.36 Å<sup>2</sup>, 98.36 Å<sup>2</sup>, 100.13 Å<sup>2</sup>, 70.67 Å<sup>2</sup>, 79.90 Å<sup>2</sup>, and 127.45 Å<sup>2</sup> for lead compounds, namely, FL04, FL05, FL07, FL09, FL10, FL11, FL12, and FL14, respectively. Water solubility property (log S) was predicted through three different models namely ESOL (-3.71, 3.31, -4.04, -4.33, -4.06, -3.53, -3.92 and -2.66), Ali (-4.5, -3.86, -5.14, -5.14, -4.87, -3.60, -4.33 and -3.21) and SILICOS-IT (-3.82, -3.82, -3.94, -5.33, -4.52, -4.98, -5.10 and -2.03). Solubility class lipophilicity refers to the capacity of a molecule to dissolve itself into a lipophilic medium and correlating to various representations of drug properties that affect ADMET including permeability, absorption, distribution, metabolism, excretion, solubility, plasma protein binding, and toxicity. Results were

assessed for ILOGP and SILICOS-IT which revealed that all compounds except FL09 (ILOGP-3.07, and SILICOS-IT 3.12) showed a most favorable range, which describes a good balance between permeability and solubility and is expected to show good bioavailability upon oral drug administration. GI absorption predicated was high for each selected molecule. Drug compounds while passing through membranes encounter various membranous barriers such as hepatocytic membrane, blood capillary walls, gastrointestinal epithelial cells, glomerulus (kidneys), blood brain barrier (BBB), and the target cell itself. This permeability foresight helps to understand the outcomes of ADMET and the cell-based bioassays. Results showed that the permeability over human skin was found to be -6.25, -6.70, -6.13, -5.99, -5.93, -6.10, -5.91, and -7.48 cm/s for compounds, FL04, FL05, FL07, FL09, FL10, FL11, FL12, and FL14, respectively. These compounds showed almost no possibility to cross the BBB except FL11. Metabolism presents an essential function in the drug-drug interaction and bioavailability of drugs. Only the free form of the drug can bind with drug-metabolizing enzymes. To study the metabolic behavior of lead compounds it is very important to study the cytochrome P450 enzymes (CYPs) as they are the most notable class of enzymes. It advocates understanding the mechanism of drug ADME,

**Table 6.** Tabular representation of predicted toxicity data of top hit flavonoid analogs.

Model Name	Units	FL04	FL05	FL07	FL09	FL10	FL11	FL12	FL14
AMES toxicity	Yes/No	No	No	No	No	No	No	No	No
Max. tolerated dose (human)	Log mg/kg/day	0.982	0.910	0.725	0.345	0.675	0.256	0.697	0.748
hERG I inhibitor	Yes/No	No	No	No	No	No	No	No	No
hERG II inhibitor	Yes/No	Yes	No	No	Yes	No	No	Yes	No
Oral Rat Chronic Toxicity (LD50)	Mol/kg	2.178	2.301	2.204	2.139	2.409	1.740	2.064	2.309
Oral rat chronic toxicity	Log mg/kg_bw/day	2.259	2.699	2.645	2.025	1.552	1.231	1.531	2.006
Hepatotoxicity	Yes/No	No	No	No	No	No	No	No	No
Skin sensitisation	Yes/No	No	No	No	No	No	No	No	No
T. Pyriformis toxicity	Log ug/L	0.352	0.345	0.290	0.303	0.337	0.778	0.518	0.300
Minnow toxicity	Log mM	0.970	1.412	1.286	0.342	0.736	1.029	-0.008	1.905

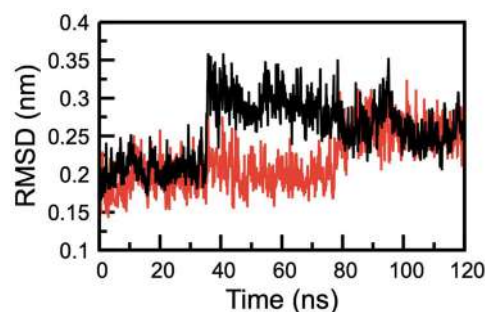
efficacy, and toxicity. To accomplish this, the top compounds found were assessed for inhibition of CYPs (CYPs of human liver microsomes (HLM)), detailed analyses are mentioned in Table 5.

### 3.3. Toxicity prediction

The identified flavonoids, FL04, FL05, FL07, FL09, FL10, FL11, FL12, and FL14 were studied in detail to explore the toxicity in-silico. Results exhibited that the **maximum tolerated dose (human)** range was between 0.256–0.982 Log mg/kg/day for all the compounds. Results revealed no hERG1 (human Ether-a-go-go-Related gene) inhibition, while three compounds (FL04, FL09, and FL12) showed hERG II inhibition. The remaining compounds may not show cardiac adverse reactions. Results did not reveal any intracellular accumulation of phospholipids (known to link with unwanted clinical side effects) as they are known to cause QT prolongation, myopathy, hepatotoxicity reaction, nephrotoxicity, and pulmonary dysfunction. None of the compounds showed hepatotoxicity and skin sensitization. All the predicted toxicity results of FL04, FL05, FL07, FL09, FL10, FL11, FL12, and FL14 molecules are mentioned in Table 6.

### 3.4. Binding pose of the docked complexes in a dynamic environment

Inspired from the results of molecular docking and ADMET analysis MD simulations of the docked complexes were performed. Molecular docking scanned the multiple conformations of the molecules and provided the energetically most preferential conformations of molecules in the active site of the target protein in the static environment. Therefore, the immobile conformational images that are generated are unable to illustrate the other important components (flexibility of residues and secondary structural elements) involved in providing stability to a protein (Bhardwaj et al., 2020). The dynamic behaviour of a protein might be affected due to the conformational changes which ultimately affect the biological functioning of the protein (Bhardwaj & Purohit, 2020). MD simulation studies are used to visualize the local/global motions and ligand induced conformations changes in a protein when in its cell-like environment. Root mean square deviation (RMSD) profile gives the idea of atomic fluctuations from the starting conformation. Stability of both docked complexes (Mpro-luteolin and Mpro-kaempferol) were evaluated by calculating the C $\alpha$  RMSD during MD run.



**Figure 7.** RMSD of backbone C-alpha atoms of complexes with luteolin (black), and kaempferol (Red).

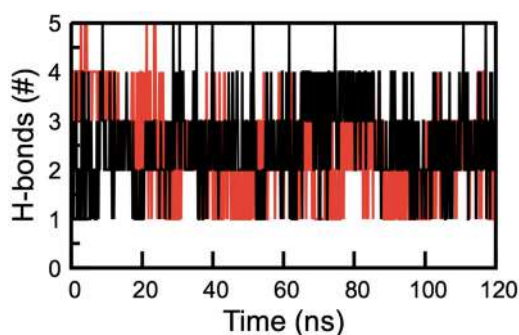
Both the protein-ligand complexes showed deviations lower than 0.4 nm (Figure 7). The average RMSD values for complexes with luteolin and kaempferol were 0.29 nm and 0.24 nm, respectively. The complex with luteolin exhibited a sharp rise in RMSD around 38 ns. However, within the 40 ns simulation time, the RMSD value comes down from 0.36 nm to 0.25 nm. On the other hand, kaempferol displayed the gradual rise in RMSD values in 70–80 ns time interval and the rest of the simulation average RMSD values remain stable  $\sim$ 0.27 nm. The protein complexes were found to be stable as is evident from the observed RMSD profile. The overall simulated structure does not exhibit any major conformational changes and remains close to the experimental structures. Further, for the confirmation of stability of the selected two molecules in the binding pocket of Mpro, structures of both the complexes were extracted at every 40 ns time intervals and various non-covalent interactions between Mpro, and luteolin and kaempferol were identified and visualized (Figures S1 and S2). Both the bioactive molecules under study stayed in the binding pocket during the course of simulation and formed many stable hydrophobic, polar and H-bond interactions as displayed in Figures S1 and S2.

### 3.5. Identification and stability of hydrogen bonds

Hydrogen bonds are one of the most important and dominant non-covalent interactions responsible for the molecular interactions between protein and ligand. It not only provides the stability of host-guest system but also the governing factor for the identification, recognition, and selectivity by conferring directionality and specificity to molecular interactions. MD simulation studies provide an ensemble of conformations in a cell-like environment of the protein. Each specific conformation of a protein has its specific interaction



pattern with the ligand. *H-bond* modules of the Gromacs were utilized to identify and monitor the evolution of a number of hydrogen bonds during the course of MD simulations for both the complexes as depicted in Figure 8. In the luteolin and kaempferol complex, the number of H-bonds fluctuates between one to five. Only a handful of conformations formed less than 2 hydrogen bonds and greater than 4 hydrogen bonds. Mpro-luteolin complex formed on an average 3 hydrogen bonds as shown in Figure 8. Mpro-kaempferol complex is involved in many transiently stable H-bonds as can be evident by the fluctuating number of H-bonds (Figure 8). It is important to mention many of the interactions that did not satisfy both the geometric criteria ( $r_{\text{HB}} \leq 0.35 \text{ nm}$  or  $\alpha_{\text{HB}} \leq 30^\circ$ ) of H-bonds and hence were classified as polar interactions. Some of the representative examples showing various non-covalent interactions between Mpro, and luteolin and kaempferol were shown in Figures S1 and S2. It is clearly evident that slight rotational and translational movement of ligand position during the simulation enhances the interactions of both the ligand with the key residues of the Mpro.



**Figure 8.** Hydrogen bond profiles of the Mpro complexes with luteolin (black), and kaempferol (red).

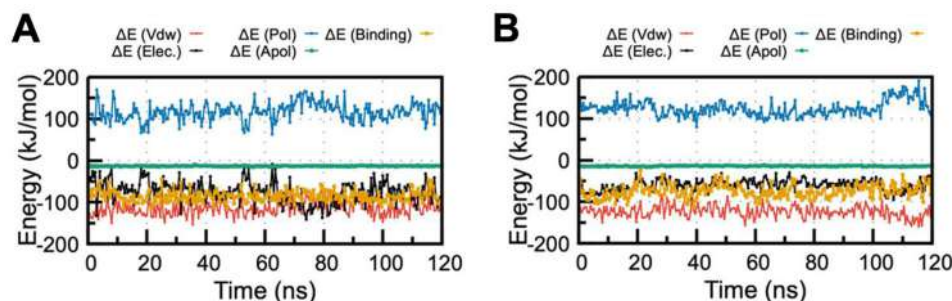
**Table 7.** Overall binding free energy and contributions from individual energy terms.

Energy (kJ/mol)	Luteolin complex	Kaempferol complex
$\Delta E_{\text{Van der Waal}}$	$-113.27 \pm 18.88$	$-123.66 \pm 13.82$
$\Delta E_{\text{electrostatic}}$	$-75.25 \pm 26.28$	$-60.47 \pm 13.39$
$\Delta E_{\text{SASA}}$	$-13.30 \pm 0.87$	$-14.28 \pm 0.98$
$\Delta E_{\text{polar solvation}}$	$116.49 \pm 21.11$	$123.92 \pm 18.06$
$\Delta E_{\text{binding}}$	$-85.34 \pm 13.57$	$-74.51 \pm 15.61$

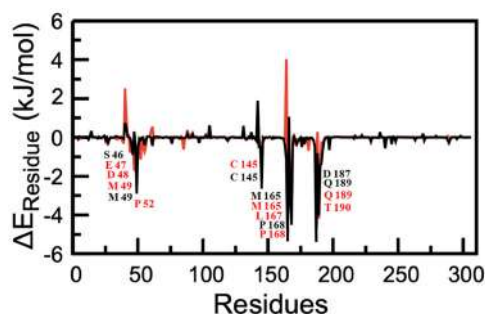
### 3.6. Binding free energy calculations

To quantify the average free binding energy of both the complexes *g\_mmpbsa* module was utilized as discussed in the method section and resultant data were summarized in Table 7. The binding free energy is the measurement of the energy released during the course of complex formation. A relatively stable protein-ligand complex displays more negative binding energy that indicates stronger affinity of the ligand towards its receptor. As discussed, in the method section binding free energy is the cumulative sum of molecular mechanics potential energy (Van der Waal and electrostatic energy) and polar and apolar (SASA) solvation energy terms. Van der Waal, electrostatic, and nonpolar solvation energy contribute favourably to the binding free energy while polar solvation energy was unfavourable in nature. Luteolin and kaempferol displayed an almost similar binding affinity with Mpro. Luteolin binds with Mpro relatively stronger with the binding affinity of  $-85.34 \text{ kJ/mol}$  while kaempferol exhibits  $-74.51 \text{ kJ/mol}$  binding free energy as summarized in Table 7.

To evaluate the contributions from individual energy components all the energy terms were plotted during the course of simulations and displayed in Figure 9. Van der Waal energy is the major governing factor for the stability of both complexes. Relatively electrostatic energy contributed more to the case luteolin that makes it a better inhibitor of the Mpro compared with the kaempferol. Furthermore, to identify the key residue of the Mpro that interacts favourably with the ligands, contributions of each residues of the Mpro in the binding free energy was decomposed. As illustrated in Figure 10, many residues contribute both favourably and unfavourably in the total binding free energy during complex formation. Although, both the complexes displayed almost similar binding affinity but a significant difference was observed in terms of contributing residues and/or their contributions. The key residues involved in the kaempferol complex were Glu47, Asp48, Met49, Pro52, Cys145, Met165, Leu167, Pro168, Asp187, Gln189, and Thr190 while in the case of luteolin the key residues involved were Met49, Cys145, His164, Met165, Leu167, Pro168, Asp187, Gln189, Thr190 and Ala191. Notable differences from the residues Met165, Pro168, Asp187 was observed. In the case of luteolin they contribute  $-5.35$ ,  $-4.51$ ,  $-5.39 \text{ kJ/mol}$  while with kaempferol their contributions significantly reduce to  $-3.55$ ,  $-2.71$  and  $-1.17 \text{ kJ/mol}$ , respectively. This observation also



**Figure 9.** MM/PBSA binding energy profile and contributions from various energy components for the (A) Mpro-luteolin and (B) Mpro-kaempferol.



**Figure 10.** Graphical representation of per residue contribution plot for luteolin (black), and kaempferol (red).

explained the slightly better affinity of luteolin over kaempferol. In earlier literature, similar residues were reported to participate with other inhibitors originated from the tea plant and FDA approved drugs (Bharadwaj et al., 2020; Bhardwaj et al., 2020). Above mentioned results clearly indicates that luteolin could have good efficacy against SARS-CoV-2 main proteases when tested experimentally. Importantly, it also has the ability to block the critical residues of the Mpro as discussed above.

#### 4. Conclusion

The number of viral infections is increasing day by day worldwide and has already created a panic situation in mankind. However, if we will investigate the current scenario, the number of deaths in the last three months because of common cold, malaria, suicidal cases, alcoholism, smoking, cancer, diabetes, and cardiovascular diseases is higher than nCOVID-19. But the biggest concern of this disease is its highly contagious nature and hence the need of the hour is to find a therapy/treatment/vaccine against the deadly SARS-CoV-2 virus. Docking results have provided us with a molecular level of understanding to conclude that the identified flavonoids namely luteolin and kaempferol are promising and might be a potential and effective inhibitor of SARS-CoV-2 as they bind in a good fashion at the active site. The ADMET study results will help in optimizing the molecules regarding their pharmacological impact. The RMSD analysis revealed that both luteolin-Mpro and kaempferol-Mpo complexes were stable to a great extent. These complexes formed a handful number of hydrogen bonds and many polar and hydrophobic contacts which reveal that such interactions provide stability of both the molecules in the binding pocket of the Mpro of SARS-CoV-2 and make them strong binder. Furthermore, MM-PBSA binding free energy calculations were used to evaluate and validate the results. Luteolin showed more favourable binding free energy compared to kaempferol. A residual level description of their binding indicates that it has the ability to block the key residues of Mpro. Hence, this study proposes luteolin as a more potent inhibitor of the Mpro of SARS-CoV-2 among all the selected flavonoids in this study. These results can contribute a significant addition to the knowledge of the full prospect of virtual screening to identify the potential hit compounds with improved potency and almost little or no toxicity.

#### Acknowledgements

We would like to express our sincere gratitude to our Department of Pharmaceutical Sciences and Technology and Department of Bioengineering, Birla Institute of Technology, Mesra (BIT-MESRA), Ranchi for providing the necessary software and support for this research work. Authors acknowledge the Department of Computer Science and Engineering, BIT-MESRA for providing a High-Performance Computing facility to carry out the Research. AJ acknowledges the Department of Biotechnology, Government of India for the Ramalingamswami Re-entry Fellowship-2019.

#### Disclosure statement

There is no conflict of interest expressed by the authors.

#### ORCID

Gourav Rakshit <http://orcid.org/0000-0003-1341-7289>  
 Pankaj Dagur <http://orcid.org/0000-0002-1084-1722>  
 Swaha Satpathy <http://orcid.org/0000-0002-2892-8957>  
 Arjun Patra <http://orcid.org/0000-0002-2761-3857>  
 Alok Jain <http://orcid.org/0000-0002-7365-7455>  
 Manik Ghosh <http://orcid.org/0000-0003-2846-2971>

#### References

- Abraham, M. J., Murtola, T., Schulz, R., Páll, S., Smith, J. C., Hess, B., & Lindahl, E. (2015). GROMACS: High performance molecular simulations through multi-level parallelism from laptops to supercomputers. *SoftwareX*, 1–2, 17–19. <https://doi.org/10.1016/j.softx.2015.06.001>
- Berendsen, H. J. C., Postma, J. P. M., Van Gunsteren, W. F., Dinola, A., & Haak, J. R. (1984). Molecular dynamics with coupling to an external bath. *Journal of Chemical Physics*, 81(8), 3684–3690. <https://doi.org/10.1063/1.448118>
- Berman, H. M., Westbrook, J., Feng, Z., Gilliland, G., Bhat, T. N., Weissig, H., Shindyalov, I. N., & Bourne, P. E. (2000). The Protein Data Bank. *Nucleic Acids Research*, 28(1), 235–242. <https://doi.org/10.1093/nar/28.1.235>
- Bharadwaj, S., Azhar, E. I., Kamal, M. A., Bajrai, L. H., Dubey, A., & Jha, K. (2020). SARS-CoV-2 Mpro inhibitors: Identification of anti-SARS-CoV-2 Mpro compounds from FDA approved drugs. *Journal of Biomolecular Structure and Dynamics*, 0, 1–16. <https://doi.org/10.1080/07391102.2020.1842807>
- Bhardwaj, V. K., & Purohit, R. (2020). Structural changes induced by substitution of amino acid 129 in the coat protein of cucumber mosaic virus. *Genomics [ Genomics*, 112(5), 3729–3738. <https://doi.org/10.1016/j.ygeno.2020.04.023>
- Bhardwaj, V. K., Singh, R., Sharma, J., Rajendran, V., Purohit, R., & Kumar, S. (2020). Identification of bioactive molecules from tea plant as SARS-CoV-2 main protease inhibitors. *Journal of Biomolecular Structure and Dynamics*, 0, 1–10. <https://doi.org/10.1080/07391102.2020.1766572>
- Chafekar, A., & Fielding, B. C. (2018). MERS-CoV: Understanding the latest human coronavirus threat. *Viruses*, 10(2).
- COVID19INDIA. (2021, Jan 27). COVID-19 [Internet]. <https://www.covid19india.org/>
- Danser, A. H. J., Epstein, M., & Battle, D. (2020). Renin-angiotensin system blockers and the COVID-19 pandemic: At present there is no evidence to abandon renin-angiotensin system blockers. *Hypertension (Dallas, TX: 1979)*, 75(6), 1382–1385. <https://doi.org/10.1161/HYPERTENSIONAHA.120.15082>
- Enmozhi, S. K., Raja, K., Sebastine, I., & Joseph, J. (2020). Andrographolide as a potential inhibitor of SARS-CoV-2 main protease: An in silico approach. *Journal of Biomolecular Structure and Dynamics*, 5, 1–7.
- Essmann, U., Perera, L., Berkowitz, M. L., Darden, T., Lee, H., & Pedersen, L. G. (1995). A smooth particle mesh Ewald method. *Journal of Chemical Physics*, 103(19), 8577–8593. <https://doi.org/10.1063/1.470117>



- Hess, B., Bekker, H., Berendsen, H. J. C., & Fraaije, J. G. E. M. (1997). LINC: A Linear Constraint Solver for molecular simulations. *Journal of Computational Chemistry*, 18(12), 1463–1472. [https://doi.org/10.1002/\(SICI\)1096-987X\(199709\)18:12<1463::AID-JCC4>3.0.CO;2-H](https://doi.org/10.1002/(SICI)1096-987X(199709)18:12<1463::AID-JCC4>3.0.CO;2-H)
- Hoffmann, M., Kleine-Weber, H., Schroeder, S., Krüger, N., Herrler, T., Erichsen, S., Schiergens, T. S., Herrler, G., Wu, N.-H., Nitsche, A., Müller, M. A., Drosten, C., & Pöhlmann, S. (2020). SARS-CoV-2 cell entry depends on ACE2 and TMPRSS2 and is blocked by a clinically proven protease inhibitor. *Cell*, 181(2), 271–280.e8. <https://doi.org/10.1016/j.cell.2020.02.052>
- Hui, D. S., Wong, P., & Wang, C. (2003). SARS: Clinical features and diagnosis. *Respirology*, 8(s1), S20–S4. <https://doi.org/10.1046/j.1440-1843.2003.00520.x>
- Jin, Z., Du, X., Xu, Y., Deng, Y., Liu, M., Zhao, Y., Zhang, B., Li, X., Zhang, L., Peng, C., Duan, Y., Yu, J., Wang, L., Yang, K., Liu, F., Jiang, R., Yang, X., You, T., Liu, X., ... Yang, H. (2020). Structure of Mpro from SARS-CoV-2 and discovery of its inhibitors. *Nature*, 582(7811), 289–293. <https://doi.org/10.1038/s41586-020-2223-y>
- Kreutz, R., Algharably, E.-H., Ganten, D., & Messerli, F. (2020). Renin-angiotensin-system (RAS) and COVID-19 to prescribe RAS blockers. *DMW - Deutsche Medizinische Wochenschrift*, 145(10), 682–686. <https://doi.org/10.1055/a-1152-3469>
- Kumari, R., Kumar, R., Lynn, A., & Open Source Drug Discovery Consortium. (2014). g\_mmpbsa-a GROMACS tool for high-throughput MM-PBSA calculations. *Journal of Chemical Information and Modeling*, 54(7), 1951–1962. <https://doi.org/10.1021/ci500020m>
- Laskowski, R. A., & Swindells, M. B. (2011). LigPlot+: Multiple ligand-protein interaction diagrams for drug discovery. *Journal of Chemical Information and Modeling*, 51(10), 2778–2786. <https://doi.org/10.1021/ci200227u>
- Li, W., Moore, M. J., Vasilieva, N., Sui, J., Wong, S. K., Berne, M. A., Somasundaran, M., Sullivan, J. L., Luzuriaga, K., Greenough, T. C., Choe, H., & Farzan, M. (2003). Angiotensin-converting enzyme 2 is a functional receptor for the SARS coronavirus. *Nature*, 426(6965), 450–453. <https://doi.org/10.1038/nature02145>
- Malde, A. K., Zuo, L., Breeze, M., Stroet, M., Poger, D., Nair, P. C., Oostenbrink, C., & Mark, A. E. (2011). An automated force field topology builder (ATB) and repository: Version 1.0. *Journal of Chemical Theory and Computation*, 7(12), 4026–4037. <https://doi.org/10.1021/ct200196m>
- Mark, P., & Nilsson, L. (2001). Structure and dynamics of the TIP3P, SPC, and SPC/E water models at 298 K. *The Journal of Physical Chemistry A*, 105(43), 9954–9960. <https://doi.org/10.1021/jp003020w>
- Matsuyama, S., Nagata, N., Shirato, K., Kawase, M., Takeda, M., & Taguchi, F. (2010). Efficient activation of the severe acute respiratory syndrome coronavirus spike protein by the transmembrane protease TMPRSS2. *Journal of Virology*, 84(24), 12658–12664. <https://doi.org/10.1128/JVI.01542-10>
- Meili, S., Jianmin, Y., Yuping, S., Guohai, S., Hospital, J. C., & Sciences, M. (2020). RAS inhibitors are one of the possible options for the treatment of new coronavirus pneumonia. *Chinese Journal of Tuberculosis and Respiratory Diseases*, 43(3), 219–222.
- Miyamoto, S., & Kollman, P. A. (1992). Settle: An analytical version of the SHAKE and RATTLE algorithm for rigid water models. *Journal of Computational Chemistry*, 13(8), 952–962. <https://doi.org/10.1002/jcc.540130805>
- Parrinello, M., & Rahman, A. (1981). Polymorphic transitions in single crystals: A new molecular dynamics method. *Journal of Applied Physics*, 52(12), 7182–7190. <https://doi.org/10.1063/1.328693>
- Pettersen, E. F., Goddard, T. D., Huang, C. C., Couch, G. S., Greenblatt, D. M., Meng, E. C., & Ferrin, T. E. (2004). UCSF Chimera—a visualization system for exploratory research and analysis. *Journal of Computational Chemistry*, 25(13), 1605–1612. <https://doi.org/10.1002/jcc.20084>
- Pires, D. E. V., Blundell, T. L., & Ascher, D. B. (2015). pkCSM: Predicting small-molecule pharmacokinetic and toxicity properties using graph-based signatures. *Journal of Medicinal Chemistry*, 58(9), 4066–4072. <https://doi.org/10.1021/acs.jmedchem.5b00104>
- Rastelli, G., DEL, R. A., Sgobba, G., & Miriam, D. (2010). Fast and accurate predictions of binding free energies using MM-PBSA and MM-GBSA. *Journal of Computational Chemistry*, 31(4), 797–810. <https://doi.org/10.1002/jcc.21372>
- Rismanbaf, A. (2020). Potential treatments for COVID-19; A narrative literature review. *Archives of Academic Emergency Medicine*, 8(1), e29. <http://www.ncbi.nlm.nih.gov/pubmed/32232214>
- Rizvi, S. M., Shazi, S., & Mohd, H. (2013). A simple click by click protocol to perform docking: Autodock 4.2 made easy for non-bioinformaticians. *EXCLI Journal*, 12, 831–857.
- Rothan, H. A., & Byrareddy, S. N. (2020). The epidemiology and pathogenesis of coronavirus disease (COVID-19) outbreak. *Journal of Autoimmunity*, 109, 102433. <https://doi.org/10.1016/j.jaut.2020.102433>
- Sawikowska, A. (2020). Meta-analysis of flavonoids with antiviral potential against coronavirus. *Biometrical Letters*, 57(1), 13–22. <https://doi.org/10.2478/bile-2020-0002>
- Sohrabi, C., Alsafi, Z., O'Neill, N., Khan, M., Kerwan, A., Al-Jabir, A., Losifidis, C., & Agha, R. (2020). World Health Organization declares global emergency: A review of the 2019 novel coronavirus (COVID-19). *International Journal of Surgery (London, England)*, 76, 71–76. <https://doi.org/10.1016/j.ijsu.2020.02.034>
- van Aalten, D. M., Bywater, R., Findlay, J. B., Hendlich, M., Hooft, R. W., & Vriend, G. (1996). PRODRG, a program for generating molecular topologies and unique molecular descriptors from coordinates of small molecules. *Journal of Computer-Aided Molecular Design*, 10(3), 255–262. <https://doi.org/10.1007/BF00355047>
- Van Der Spoel, D., Lindahl, E., Hess, B., Groenhof, G., Mark, A. E., & Berendsen, H. J. C. (2005). GROMACS: Fast, flexible, and free. *Journal of Computational Chemistry*, 26(16), 1701–1718. <https://doi.org/10.1002/jcc.20291>
- Weis, A., Katebzadeh, K., Söderhjelm, P., Nilsson, I., & Ryde, U. (2006). Ligand affinities predicted with the MM/PBSA method: Dependence on the simulation method and the force field. *Journal of Medicinal Chemistry*, 49(22), 6596–6606. <https://doi.org/10.1021/jm0608210>
- Williams, C. J., Headd, J. J., Moriarty, N. W., Prisant, M. G., Videau, L. L., & Deis, L. N. (2017). MolProbity: More and better reference data for improved all-atom structure validation. *Protein Science*, 27(1), 293–315. doi:10.1002/pro.3330
- World Health Organization. (2021, Jan 27). WHO Coronavirus Disease (COVID-19) Dashboard (2020). [Internet]. [https://covid19.who.int/?gclid=Cj0KCQiAqo3-BRDoARIsAE5vnaLUkiwOHsg4XguCRXHirZbiEkudrGr2gqiqItLCFBV9sValQUHtfhcUaAv1fEALw\\_wcB](https://covid19.who.int/?gclid=Cj0KCQiAqo3-BRDoARIsAE5vnaLUkiwOHsg4XguCRXHirZbiEkudrGr2gqiqItLCFBV9sValQUHtfhcUaAv1fEALw_wcB)
- Yang, T., Chen, Y.-Y., Liu, J.-R., Zhao, H., Vaziri, N. D., Guo, Y., & Zhao, Y.-Y. (2019). Natural products against renin-angiotensin system for anti-fibrosis therapy. *European Journal of Medicinal Chemistry*, 179, 623–633. <https://doi.org/10.1016/j.ejmech.2019.06.091>
- Zakaryan, H., Arabyan, E., Oo, A., & Zandi, K. (2017). Flavonoids: Promising natural compounds against viral infections. *Archives of Virology*, 162(9), 2539–2551. <https://doi.org/10.1007/s00705-017-3417-y>
- Zhou, P., Yang, X.-L., Wang, X.-G., Hu, B., Zhang, L., Zhang, W., Si, H.-R., Zhu, Y., Li, B., Huang, C.-L., Chen, H.-D., Chen, J., Luo, Y., Guo, H., Jiang, R.-D., Liu, M.-Q., Chen, Y., Shen, X.-R., Wang, X., ... Shi, Z.-L. (2020). A pneumonia outbreak associated with a new coronavirus of probable bat origin. *Nature*, 579(7798), 270–273. <https://doi.org/10.1038/s41586-020-2012-7>